Netsu Sokutei **19** (3) 135-144

総　説

Thermochemical Data and Software for the Optimization of Processes and Materials

E. Königsberger, E. Schuster, H. Gamsjäger,
C. God*, K. Hack**, M. Kowalski** and P. J. Spencer**

(Received April 13, 1992)

Computer assisted thermochemistry is nowadays a tool that can be applied in many fields. Provided the thermochemical data, i.e. the Gibbs energy as function of temperature, and for solution phases also of composition, are known for all possible phases of a chemical system, the Gibbs energy minimization techniques available today allow rapid and reliable calculation of complex equilibrium states. Several applications of the program ChemSage are discussed to give a better understanding of the general scope of computer assisted thermochemistry. The examples cover such different cases as salt production from brines, combustion equilibria with heat balances, the avoidance of clogging problems in continuous casting of steels and the optimization of hard-facing alloy.

1. Introduction

The calculation of thermochemical equilibrium states is the basis for the solution of many problems in process engineering or materials science. The calculations are carried out by minimization of the Gibbs energy of the system under consideration taking proper account of the global parameters system composition, temperature and total pressure. One of the most up-to-date computer programs for this purpose is ChemSage[1]. In conjunction with critically evaluated thermochemical data this program permits a reliable description and, in consequence, optimization of process variants or materials properties. Several examples will be given below. It is worth noting that although these examples stem from very different technical fields the general approach to the problem solving is the same in all cases because of the same underlying physico-chemical principles.

Abteilung für Physikalische Chemie und Theoretische Hüttenkunde, Montanuniversität Leoben, A-8700 Leoben, Austria

* Institut für Wärmetechnik, Industrieofenbau und Energiewirtschaft, Montanuniversität Leoben, A-8700 Leoben, Austria

** Lehrstuhl für Theoretische Hüttenkunde, RWTH Aachen, D-5100 Aachen, Germany

2. Chemical Aspects of Common-Salt Production

E. Königsberger, and H. Gamsjäger

2.1 Purification of Rock-Salt Brines

In Austria sodium chloride is extracted from rock-salt deposits by water resulting in brines, the starting material for common-salt production. These brines are essentially saturated with NaCl but contain also various other salts which on the one hand interfere with the evaporation process (scale formation on heat exchangers and boilers) and are on the other hand undesired impurities in the NaCl produced. In particular, alkaline earth compounds have to be removed from the original brines.

The "Österreichische Salinen AG" employs the so-called "Schweizerhalle" purification process which operates discontinuously by two steps:

1. The brine is reacted with calcium oxide (CaO) and SO_4^{2-}-rich mother liquor (from the evaporation process), thereby most of the Mg^{2+} ions are removed as brucite ($Mg(OH)_2$) and part of the Ca^{2+} ions are precipitated as gypsum ($CaSO_4 \cdot 2H_2O$).
2. The carbonization of excess OH^- ions with flue gas containing about 12 vol.-% CO_2 results in precipitation of

calcium carbonate ($CaCO_3$). The remaining Ca^{2+} ions will finally be removed by addition of sodium carbonate (Na_2CO_3).

With respect to economy and environmental protection it is of obvious importance to optimize this process. This Austrian brine purification process has been discussed recently[2], however, the thermodynamic considerations and calculations with ChemSage[1] apply for analogous processes and are reported here.

2.1.1 Thermochemical model

The Pitzer model[3] and the data base of Harvie *et al.*[4] containing about 50 stoichiometric phases and 130 ion-interaction parameters were used to calculate phase equilibria in the system Na^+-K^+-Mg^{2+}-Ca^{2+}-H^+-Cl^--SO_4^{2-}-OH^--HCO_3^--CO_3^{2-}-CO_2-H_2O at 25°C.

Three aspects concerning the data base and the thermodynamic assumptions of the present calculations should be emphasized:

1. For the subsystem $NaCl$-$CaSO_4$-H_2O the parameters of Harvie and Weare's[5] older compilation were retained, because they modeled the solubility of gypsum in NaCl brines more accurately.
2. Anhydrite has been found to be more stable than gypsum in saturated NaCl solutions at 25°C (*cf.*[6]) which is also predicted by these thermodynamic data[5]. It is well known, however, that anhydrite precipitation is often kinetically retarded and consequently a metastable equilibrium between gypsum and solution is attained. This was modeled with ChemSage by suppressing the stable phase anhydrite, and in fact precipitation of gypsum from saturated NaCl brines is observed in the present industrial process[7].
3. Aragonite, which is less stable than calcite, is reported to be formed in the second step[7]. This is a peculiar result because Mg^{2+}, which has a retarding effect on calcite precipitation, should have been essentially removed in the first step. However, the stable phase calcite was suppressed and calculated aragonite solubilities (which are higher than calcite solubilities by a factor of 1.5 at the sodium carbonate molalities applied) agree well with Ca^{2+} molalities obtained experimentally.

In this way it was possible to predict the optimal amounts of calcium oxide, flue gas, and sodium carbonate which have to be added to the original brine when the "Schweizerhalle" process is carried out.

2.1.2 Process optimization

Starting from a typical brine composition[7], Fig. 1a shows the effect of CaO additions on Mg^{2+} and OH^- molalities and the amount of gypsum formed in the first step. It turned out that it is advantageous to saturate the brine with portlandite ($Ca(OH)_2$) because CaO is a considerably cheaper base than sodium carbonate (line C, Figs. 1c, 1f, and 1g). However, in the alternative process starting from line B (Figs. 1b, 1d, and 1e) about 10% less gypsum and calcium carbonate is formed.

As shown in Figs. 1b and 1c, "back-titration" of OH^- with CO_2 from flue gas results in the typical sigmoidal pH curves. It is, however, preferable to discontinue the CO_2 addition before the equivalence point is reached (line F) because, as indicated in Figs. 1f and 1g, the HCO_3^- molality is then lower and consequently extensive frothing can be avoided in the evaporation step. Moreover, the brucite precipitate can never be quantitatively removed in the first step, therefore, an OH^- molality lower than about 2 to 3 mmol·kg^{-1} leads to an unacceptable increase in $[Mg^{2+}]$. Fig. 2 indicates experimental results of the "Österreichische Salinen AG" compared with brucite solubilities calculated according to Harvie *et al.*[4] (solid line) and our own assessment[8] (dashed line). It has to be noted, however, that Harvie's μ^θ values and ion-interaction parameters are interrelated and thus changing one quantity ($\mu^\theta_{brucite}$) without adjusting the others should be performed with care. Nevertheless, compared to the experimental scatter, the Mg^{2+} content of purified brines can be predicted reasonably well.

To sum up, the process indicated by the lines C-F-H, which is employed by the "Österreichische Salinen AG", is optimal under the prevailing circumstances. However, alternatives suggested by changing economical and legislative restrictions could be modeled reliably.

2.2 Salt production by Evaporation

The highly soluble salts thenardite (Na_2SO_4) and sylvite (KCl) cannot be removed by the "Schweizerhalle" process described. Crystallization of these salts together with NaCl must be avoided when the brine is boiled down at atmospheric pressure.

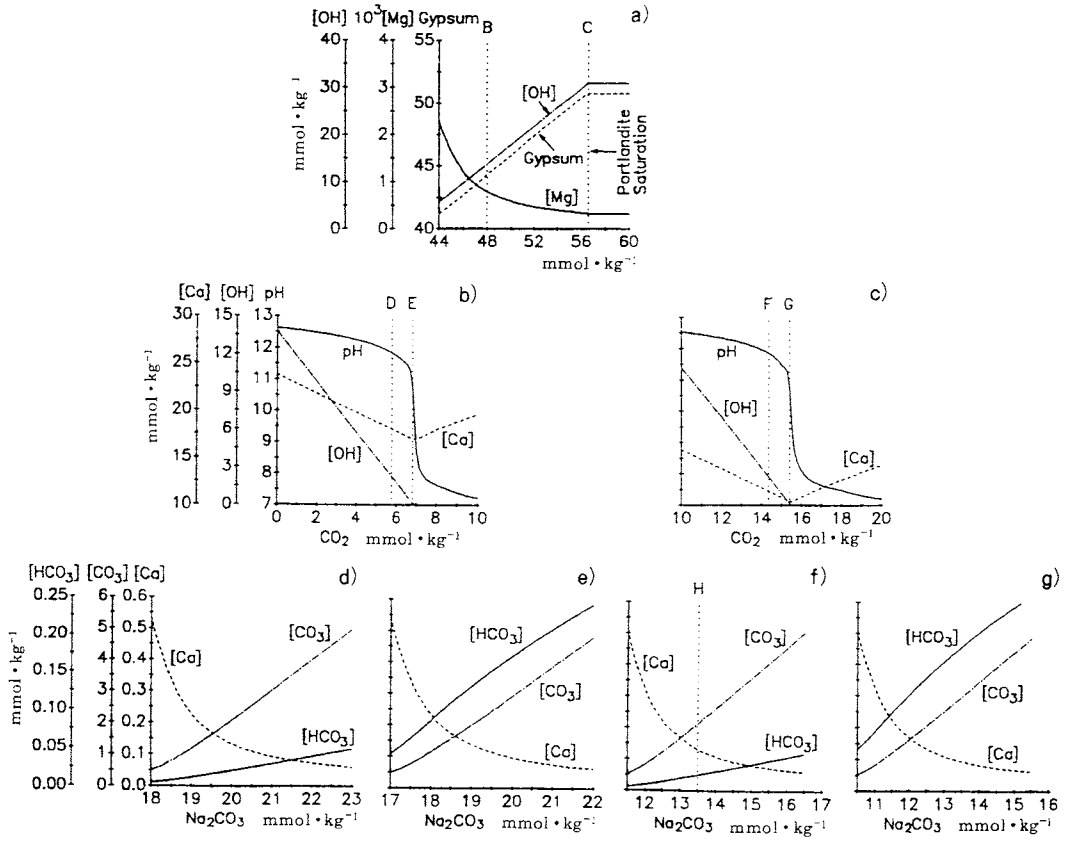

Fig. 1 Purification of rock-salt brines according to the "Schweizerhalle" process.
a) Precipitation of brucite and gypsum with lime. b), c) Carbonization with flue gas. d) – g) Final Ca^{2+} precipitation with sodium carbonate. The ordinate captions refer to all figures in a row. The different processes (dotted lines) are described in the text.

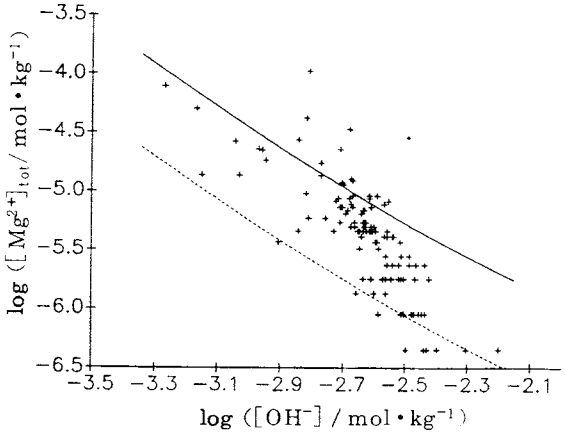

Fig. 2 Solubility of brucite in purified brines.
Solid line: Calculated from parameters of Harvie *et al.*[4]. Dashed line: $\mu^{\theta}_{brucite}$ from ref. 8+Experimental[7].

2.2.1 Phase diagram of the system Na^+-K^+-Cl^--SO^{2-}-H_2O

A recently published model[9] allows the calculation of solubilities in the system Na^+-K^+-Cl^--SO^{2-}-H_2O in the temperature range 0 to 250°C. The temperature dependence of solubility products and Pitzer parameters is given[9] by the empirical 8-parameter expression

$$f(T) = a_1 + a_2T + a_3/T + a_4\ln T + a_5/(T - 263) + a_6T^2 + a_7/(680 - T) + a_8/(T - 227). \quad (1)$$

However, ChemSage uses functions

$$G(T)/RT = g_1 + g_2T + g_3/T + g_4\ln T + g_5/T^2 + g_6T^2 \ldots \quad (2)$$

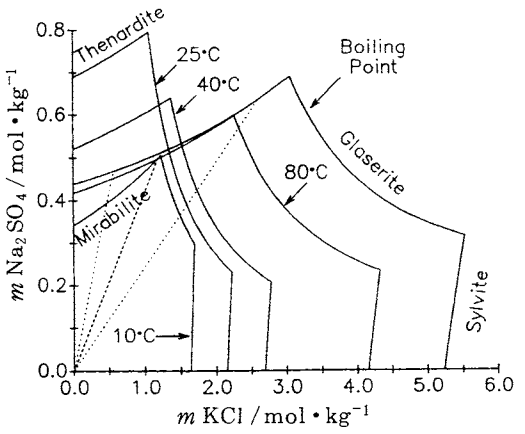

Fig. 3 Phase diagram of the system Na^+-K^+-Cl^--SO_4^{2-}-H_2O at NaCl saturation.
Dotted lines: Compositional range of purified brines. Dashed line: Mean value in 1990[7].

Consequently, original μ^θ/RT functions (1) were refitted in the temperature range 0 – 150°C to the 6-parameter function (2). Pitzer parameters were refitted to a 4-parameter expression (Eq. 2, g_1 ... g_4), because ChemSage allows a maximum number of 4 parameters describing the temperature dependence of excess functions. Deviations of refitted functions from original ones were negligible for the present solubility calculations. The phase diagram KCl-Na_2SO_4-H_2O at NaCl saturation calculated for various temperatures is shown in Fig. 3. Boiling points of these brines are about 108°C at an external pressure of 0.95 atm.

2.2.2 Conclusion

For typical compositions of purified brines[7], the evaporation process is limited by the solubility of thenardite, which decreases with increasing temperature to a minimum at about 80°C. Mirabilite ($Na_2SO_4 \cdot 10\ H_2O$) is only stable below 19°C. In K^+-rich brines, glaserite ($Na_2SO_4 \cdot 3\ K_2SO_4$) may be formed at cooling; however, when $[K^+]/[SO_4^{2-}] \leq 2.5$, pure NaCl should precipitate.

3. Thermodynamic Calculations of Combustion Reactions

E. Schuster, H. Gamsjäger and C. God,

3.1 Composition of Flue Gas

The composition of flue gases is an important criterion of the efficiency achieved in combustion reactions and provides the basis for calculations of adiabatic combustion temperatures. Often it is assumed that the carbon and hydrogen content of the fuel is quantitatively oxidized by oxygen resulting in CO_2 and H_2O, while nitrogen from air (and fuel) remains in molecular form. At high temperatures this assumption is no longer justified.

The decomposition of CO_2 and H_2O as well as the formation of NO_x are simultaneously occurring side reactions, which complicate the numerical treatment. There are well known graphical and numerical approximations[10),11)], by which the degree of decomposition can be calculated depending on temperature and air ratio, n (= amount of air present/amount of air stoichiometrically sufficient), however, these methods are applicable only for a limited number of components and restricted to the accuracy inherent to geometrical constructions.

With ChemSage[1)] all known reactions occurring in combustions can simultaneously be taken into account. As usual the calculations start from the assumption that chemical equilibrium will be attained, which is certainly justified at high temperatures. Gibbs functions ($\Delta_f G^\theta_i$) of all relevant combustion products, i, serve as the necessary and sufficient data base. It does not matter when thermodynamic data of the fuel are lacking, provided it is completely consumed during the combustion and consequently not contributing to the Gibbs functions of the reaction products. In fact the equilibrium composition of the flue gas can be calculated once the chemical analysis of the fuel and the air is known (Fig. 4).

3.2 Adiabatic Combustion Temperatures

An important quantity is the adiabatic-combustion temperature, which varies with the fuel and the starting conditions. Several methods have been proposed to calculate this quantity (see *e.g.* refs. 12, 13), however, in any of these cases simplifying assumptions are necessary. Consequently, by nomographical methods and $H - t$ diagrams* theoretical combustion temperatures can at best be predicted within ±10 K, due to neglected side reactions and graph reading errors.

When these calculations are performed with Chem Sage only the enthalpy of formation of the fuel has to be included

* Whereas the symbol H for enthalpy is recommended by IUPAC, in the technical literature I is often encountered instead.

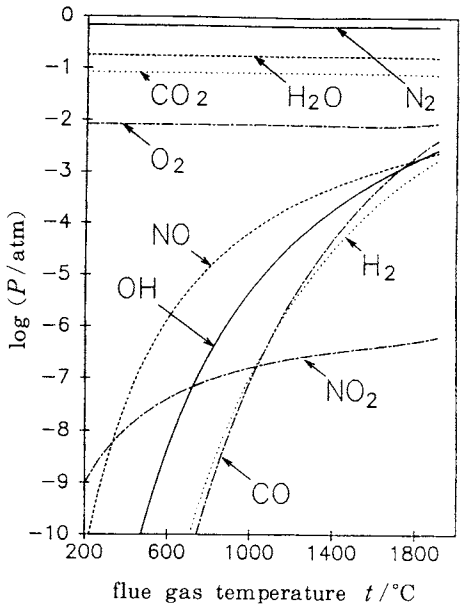

Fig 4 Combustion of natural gas; flue gas composition. Continental natural gas was burned at an air ratio of n = 1.05 and a relative humidity (t_{air} = 25°C) of 60%. Composition of a continental natural gas (January 91): component/vol.-%; CH_4/97.20; C_2H_6/0.78; C_3H_8/0.22; C_4H_{10}/0.24; CO_2/0.62; N_2/0.94.

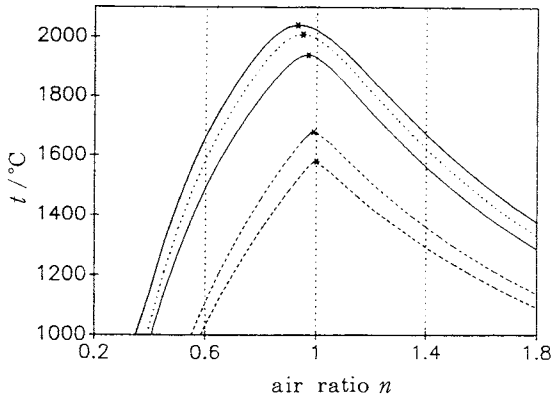

Fig. 5 Adiabatic combustion temperatures of several fuels (from above to below: hard coal (for power stations), fuel oil, natural gas, wood chips and soft coal (raw)) at p = 946 mbar, t_{air} = 10°C and 60% relative humidity.

into the data base of section 1. The necessary information can easily be obtained from the experimentally determined enthalpy of combustion. With this method the adiabatic combustion temperatures have been calculated as functions of the air ratio for various solid, liquid and gaseous fuels (Fig. 5). Note, that the maximum temperature of combustion is obtained at $n \leq 1$.

Conventional approximation methods are rather time consuming and typically take several hours to obtain the desired result, whereas with ChemSage it is a matter of several minutes.

At constant air ratios it turned out that good correlations exist between the enthalpy of combustion $\Delta_r H_{(\text{flue gas})}$ (referring to 1 mol flue gas produced during combustion with air) and the adiabatic temperature t_{ad}. When the enthalpy of combustion, the elemental composition of the fuel, and the air ratio n are known, t_{ad} can be estimated within ±50°C using Eq. (3):

$$t_{ad}/°C = 583 - 1045 \cdot (n - 1) + 17.5 \cdot \Delta_r H_{(\text{flue gas})}/\text{kJ mol}_{(\text{flue gas})}^{-1} \quad (3)$$

This is certainly the fastest way to obtain approximate adiabatic combustion temperatures when the program ChemSage is not available.

4. Avoidance of Deposits in Submerged Nozzles during Continuous Casting of Steel

P. J. Spencer and K. Hack

For some time now, "nozzle-clogging" during continuous casting of steel has been a much-discussed problem[14)-16)]. The growth of solid deposits on the walls of the submerged nozzles results in a gradual clogging, and the possible danger of breaking off of larger particles. These may be trapped in the solidifying cast. As a result, the nozzles must be changed frequently.

Aluminium is a grain-refiner in steel and for this reason is an alloying addition in many high-grade steels. However, there is an associated tendency to form alumina deposits in the submerged nozzles. Attempts are being made to reduce the problem by flushing with argon or using ceramic filters[17),18)]. Addition of calcium has also proved useful in forming low-melting calcium-aluminates. Nevertheless, for grades containing >0.05% S to improve machinability, sulphide deposits can form despite treatment with calcium.

The following thermodynamic equilibrium considerations in the system Fe-Al-Ca-O-S examplify the possible processes occurring. For this purpose, only the most important components and phases in characteristic temperature and composition ranges are considered. The conditions for the equilibrium calculations are as follows:

Components: Fe, Ca, Al, O, S
Phases: Metal(l), Oxide(l), xCaO · yAl$_2$O$_3$, Sulphide
Global conditions: T fix, variable O and Ca content in Fe(l)

4.1 Thermochemical Basis

The program ChemSage[1] was used to calculate the equilibria. It determines the equilibrium state by minimization of the Gibbs energy of the system taking into account the mass-balance of the individual components of the system. A suitable Gibbs energy description is selected for each phase, here:

1. Metal(l)
   Dilute metallic solution using the
   Pelton and Bale[19]
   modification of the Wagner description.
   Components: Fe, Al, Ca, O, S

2. Oxide(l)
   Oxide melt using Gaye's extension[20] of the Kapoor and Frohberg cell model.
   Components: CaO, Al$_2$O$_3$

3. xCaO·yAl$_2$O$_3$
   All calcium aluminates and solid CaO and Al$_2$O$_3$ as pure stoichiometric phases.

4. Sulphide
   Sublattice model due to Sundman and Ågren[21].
   Components: CaS and FeS

This procedure ensures a self-consistent data set for the Fe-Al-Ca-O-S system in the iron-rich corner. At the same time the subsystem Al$_2$O$_3$-CaO is treated in its entirety (Fig. 6)[22]. Going across the figure at a constant temperature, *e.g.* 1600°C, shows which phase(s) can possibly precipitate from the iron melt.

The equilibria for the entire system are illustrated in Fig. 7, together with experimental results from the literature[23]. The total concentrations of Ca and O in the system are the axis variables and the total Al and S contents are fixed parameters. The temperature was chosen to be 1600°C.

4.2 Conclusions

Fig. 7 clearly illustrates that for particular conditions a socalled "window" exists within which only a liquid oxide phase is formed from the metallic melt constituents. This

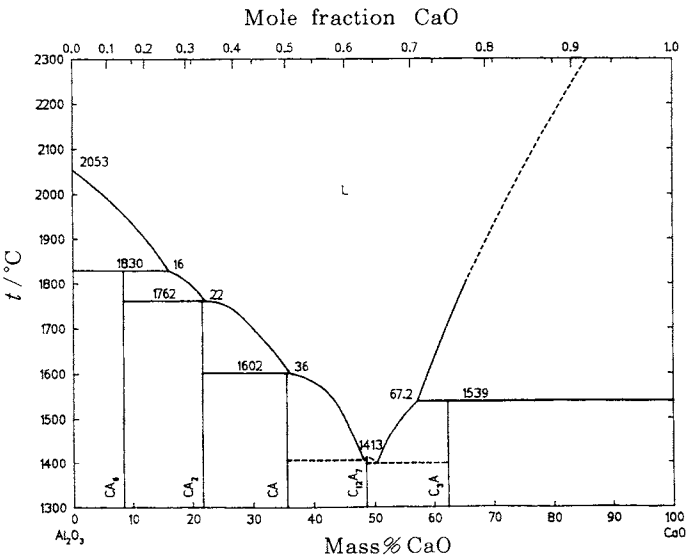

Fig. 6 Phase diagram of the subsystem CaO - Al$_2$O$_3$[22]

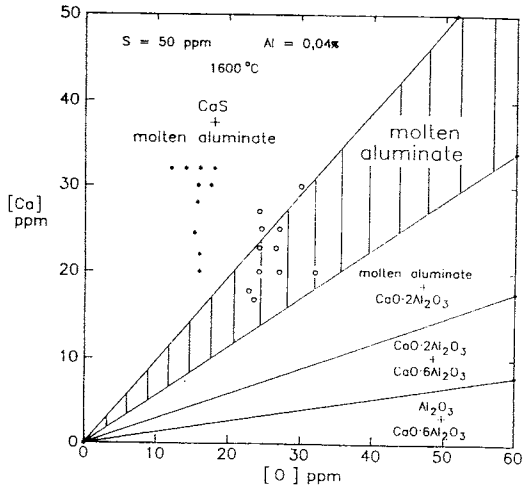

Fig. 7 The calculated slag window with experimental results by Pellicani[23]
* CaS found ° no CaS found

does not produce deposits in the submerged nozzles. However, if the calcium content at a given oxygen content is too low, solid calcium aluminates can form in the sequence illustrated in Fig. 6. At high Ca-contents, a solid sulphide precipitate can form together with the liquid oxide.

The "nozzle-clogging" problem is illustrated here only with an example calculation. This shows however, that thermochemical measures (control of composition and temperature of the Fe-bath) are themselves capable of allowing the problem to be avoided. The calculations can be refined by consideration of further components and variation of system parameters, *e.g.* temperature, which give closer simulation of the conditions encountered in practice.

5. Optimization of Wear Resistant Hard-Facing Alloys

M. Kowalski, K. Hack and P. J. Spencer

Hardfacing alloys have found widespread use in prolonging the lifetime of parts of digging and transportation equipment in energy and ore production which undergo heavy mineral abrasive wear. Mostly, Fe-Cr-C alloys are used. These are of a composition such that the range of M_7C_3 primary solidification is reached.

The chromium content necessary to obtain the desired structures and properties of the wear resistant layers is fairly high (> 20 wt%). Considering the fact that this amount of chromium is lost completely through abrasion, it is reasonable to search for a cheaper replacement.

The influence of several different alloying elements on the structure and the wear resistance of Fe-Cr-C alloys has been studied for some time. In particular, the possibility of replacement of chromium by boron and silicon has been investigated[24),25]. These investigations made clear that boron mainly acts as an agent for the formation of hard (boride) phases and thus essentially replaces carbon[24]. However, it could be shown[25] that silicon satisfies most of the requirements of a chromium replacement.

Silicon dissolves in the matrix and thereby influences favourably the compositions and amounts of hard phases. Too high a content of silicon, however, leads to embrittlement of the iron matrix as a result of ordering phenomena.

In the present work, the influence of silicon on the syste system Fe-Cr-C has been studied by means of abrasion experiments, metallographic investigation and thermodynamic equilibrium calculations. The compositions have been chosen such the Cr to C weight ratio was always egal to 5 and the silicon content up to 10 wt%.

5.1 Sample Preparation, Abrasion Experiments and Equilibrium Calculations

All alloys investigated were melted under argon in a Tamman furnace and solidified in steel ingots. The sample and ingot measures have been chosen such that the cooling conditions yielded a macro- and micro-structure which resembles closely those of a hard-facing alloy. After the abrasion runs the samples were investigated qualitatively and quantitatively by conventional light microscopy.

The abrasion experiments were carried out in a Harworth apparatus (Fig. 8), which reproduces best the conditions of mineral abrasive wear as they occur in practice.

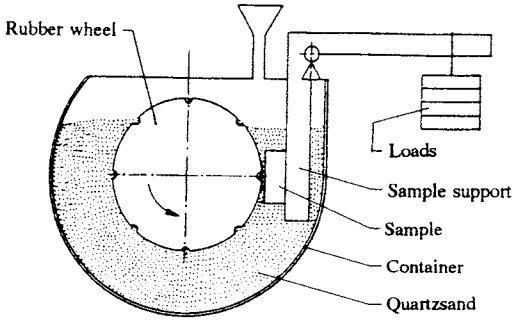

Fig. 8 Schematic drawing of a Harworth-apparatus

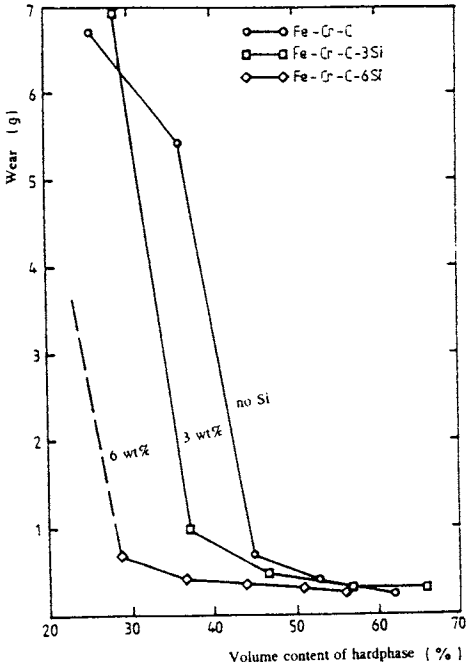

Fig. 9 Influence of Silicon on the abrasive wear of Fe-Cr-C-alloys

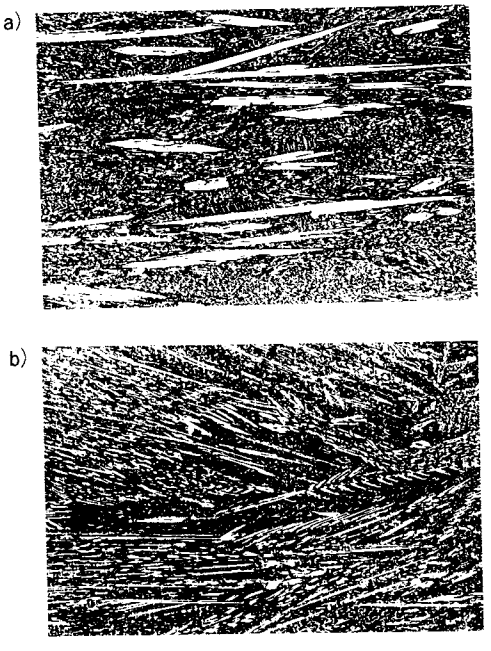

Fig. 10 Hyper-eutectic structures (magnification: 100)
a. 4.3 wt% C, 21.6 wt% Cr, no Si
b. 3 wt% C, 15 wt% Cr, 6 wt% Si

The thermochemical equilibrium calculations in the multicomponent multiphase system Fe-Cr-C-Si were carried out using ChemSage[1]. As a complete dataset for the system did not exist in the literature, it was necessary to assess the missing parameters prior to carrying out the required equilibrium calculations.

5.2 Wear and Structure

The results of the abrasions experiments are given in Fig. 9, which shows the total amount (in gram) of material loss as a function of the volume contents of hard phases in the sample. Analogous to the behaviour of Fe-Cr-C and Fe-Cr-C-B hard-facing layers[26), 27] a sigmoidal dependence with a sharp change from relatively high abrasion to good wear-resistance is found. As in the case of the afore-mentioned alloys, this is caused by a change from hypo- to hypereutectic structure.

Figs. 10a and 10b show, for example, hypereutectic structures. 21.6 wt% Cr are necessary when no silicon is added, but only 15 wt% Cr with 6 wt% of Si. This can be explained by a shift of the eutectic valley in silicon-containing alloys. The calculated liquidus surfaces for different silicon contents are shown in Figs. 11a – 11c.

5.3 Calculated Phase Diagrams

To obtain a more complete picture of the influence of Si on the position of the eutectic valley and the more complex phase relations in the sub-solidus range, the dataset mentioned above has been used in extensive equilibrium calculations employing the program ChemSage[1]. This program permits the choice of the conditions of an equilibrium such that even for a multicomponent, multiphase system, quantitative two-dimensional representations are possible.

Fig. 12 shows such isotherms for the system Fe-Cr-C with up to 10 wt% C and with addition of 0, 3 and 6 wt% Si respectively. The temperature (1200°C) was chosen such that no liquid is formed. From the diagrams it is obvious that the addition of silicon will cause considerably more complex phase relationships even for low chromium and carbon contents.

The primary solidification ranges of the hard phases which are especially important for the hardfacing procedure are shown in Fig. 11, in which the calculated liquidus surface is given. As mentioned above the positive influence of silicon can be recognized, as the range of primary solidification of the M_7C_3 phase is shifted towards lower Cr-

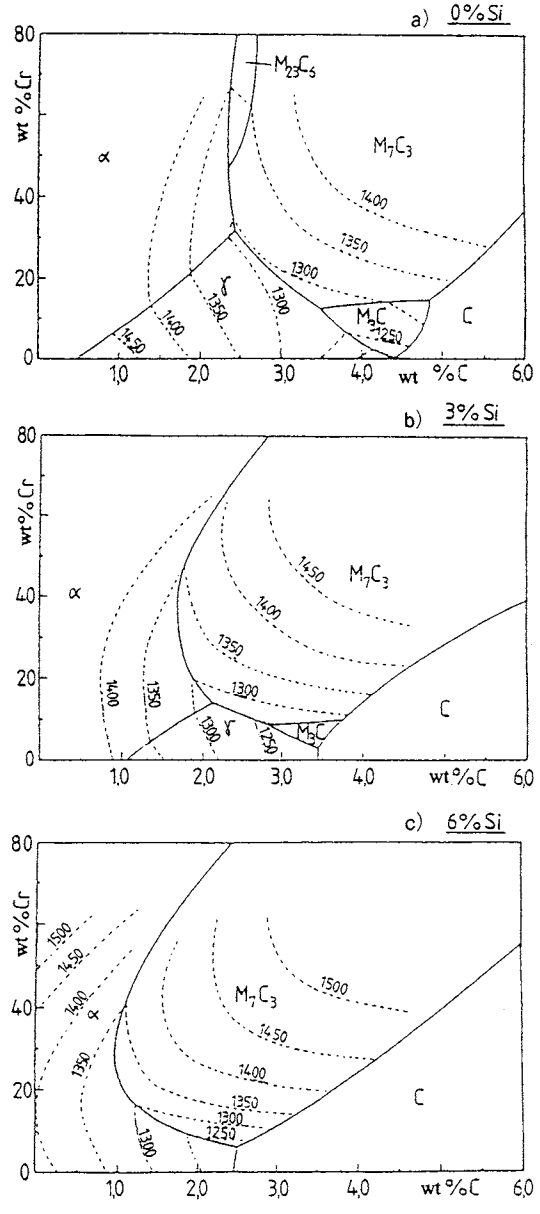

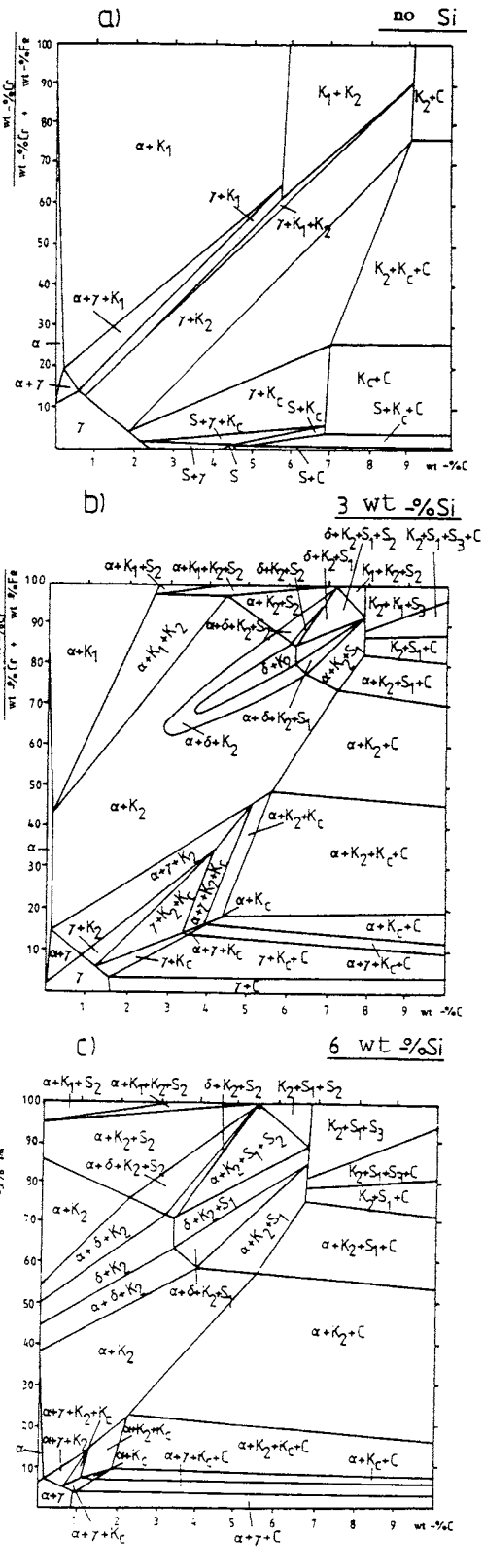

Fig. 11 Influence of Silicon on the eutectic valley as calculated from thermodynamic data

Fig. 12 Influence of Silicon on the phase formation of Fe-Cr-C-alloys at 1200°C

a. no Si

b. 3 wt% Si

c. 6 wt% Si

$K_1=M_{23}C_6$, $K_2=M_7C_3$, $K_c=M_3C$, $S_1=M_5Si_3$, $S_2=Cr_3Si$, $S_3=SiC$

and C-contents. On the other hand, the diagram also shows clearly the limit for the reduction of the chromium content, as this will cause pure graphite to precipitate, thereby causing a deterioration of the wear-resistance.

6. General Summary

The present contribution shows how carefully chosen thermochemical data in conjunction with the computer program ChemSage can assist in the understanding of processes in aqueous electrolytes and in steel metallurgy. Furthermore it is demonstrated that the same software can also be employed in combustion calculations or for the understanding of phase relations in hard-metal alloys. In all cases rapid and reliable answers for multicomponent, multiphase equilibria could be obtained.

This paper indicates only some of the possibilities for calculations with ChemSage. Further applications include, *e.g.* the calculation of geochemical high-temperature, high-pressure equilibria[28] as well as the simulation of multi-staged con- or counter-current flow reactors[29]. ChemSage is thus a universal tool for the solution of thermochemical problems.

References

1) G. Eriksson, K. Hack, *Metall. Trans B* **21B**, 1013 (1990).
2) K. Hack, M. Kowalski, P. J. Spencer, E. Königsberger, E. Schuster, H. Gamsjäger and C. God, *Berg- und Hüttenmänn. Monatsh.* **136**, 417 (1991).
3) K. S. Pitzer, *J. Phys. Chem.* **77**, 268 (1973).
4) C. E. Harvie and N. Moller, J. H. Weare, *Geochim. Cosmochim. Acta.* **48**, 723 (1984)
5) C. E. Harvie and J. H. Weare, *Geochim. Cosmochim. Acta.* **44**, 918 (1980).
6) C. W. Blount and F. W. Dickson, *Am. Mineral.* **58**, 323 (1973).
7) Österreichische Salinen AG, personal communication, (1990).
8) E. Königsberger, P. Schmidt and H. Gamsjäger, *J. Solution Chem.*, submitted for publication, (1992).
9) J. P. Greenberg and N. Moller, *Geochim. Cosmochim. Acta.* **53**, 2503 (1989).
10) E. Schwarz - Bergkampf, *Z. Anorg. Allg. Chem.* **206**, 317 (1932).
11) E. Schwarz - Bergkampf, *High Temperature - High Pressure* **10**, 667 (1978).
12) E. Schwarz - Bergkampf, *Radex-Rundschau* **1951**, 265
13) H. Schöberl, *Gaswärme Int.* **6**, 351 (1957).
14) S. N. Singh, *Metall. Trans B* **5B**, 2165 (1974).
15) H. M. Pielet and D. Bhattachary, *Metall. Trans B* **15B**, 547 (1984).
16) A. Ishii, A. Shikawa and Y. Nakamura, *Interceram* (spec. iss.) **36**, 70 (1987).
17) K. Umezawa and Y. Nuri, *Tetsu to Hagane* **75**, 1829 (1989).
18) F. Höfer, P. Patel and H. J. Selenz, *Stahl und Eisen* **110**, 131 (1990).
19) C. W. Bale and A. Pelton, *Metall. Trans. A* **12A**, 1997 (1990).
20) H. Gaye and J. Welfringer, Metall. Slags Fluxes, 2. Int. Symp. Proc., 357 (1984).
21) B. Sundman and J. Agren, *J. Phys. Chem. Sol.* **42**, 297 (1981).
22) M. Kowalski, new edition of Slag Atlas, private communication, RWTH Aachen, (1990).
23) F. Pellicani, F. Villette and J. Dubois, *Scan.* Inject 4, Lulea, Sweden, June 11 – 13, Paper No. 29 (1986).
24) H. Drzeniek, M. Kowalski, K. Granat and E. Luggscheider, *Sonderbände der Praktischen Metallographie* **20**, 353 (1989).
25) K. Granat, Dissertation, RWTH Aachen, (1989).
26) H. Koch and E. Bernnholz, *Schweißen und Schneiden* **120**, 75 (1958).
27) M. Kowalski, K. Granat, H. Drzeniek and E. Lugscheider, unpublished, RWTH Aachen, Lehr- und Forschungsgebiet Werkstoffeigenschaften, (1989).
28) Y. Fei and S. K. Saxena, *Phys. Chem. Minerals* **13**, 311 (1986).
29) T. Johansson and G. Eriksson, *J. Electrochem. Soc.* **131**, 365 (1984).

要　旨

コンピュータ支援による熱化学計算は，近年種々の分野で研究手段のひとつとして用いられるようになってきた。問題となる系に含まれる各相の自由エネルギーの温度ならびに組成依存性などの熱力学データが与えられると，自由エネルギの最小値を迅速かつ精度よく求める計算手法を用いて，複雑な相平衡関係を計算できる。本稿では，Chem Sageという化学平衡計算ソフトウエアを用いて行なった種々の計算例を紹介する。